Research Article | Vol. 26, No. 25 | 10 Dec 2018 | OPTICS EXPRESS 33245
Optics EXPRESS

Fabrication of hybrid Fabry-Pérot microcavity using two-photon lithography for single-photon sources

F. ORTIZ-HUERTA,[1,*] L. CHEN,[1] M. TAVERNE,[1] J. P. HADDEN,[3] M. JOHNSON,[1,2] Y. L. D. HO,[1] AND J. G. RARITY[1]

[1]*Quantum Engineering Technology Labs, H. H. Wills Physics Laboratory and Department of Electrical and Electronic Engineering, University of Bristol, Bristol BS8 1FD, UK*
[2]*Quantum Engineering Centre for Doctoral Training, H. H. Wills Physics Laboratory and Department of Electrical and Electronic Engineering, University of Bristol, Tyndall Avenue, BS8 1FD, UK*
[3]*School of Physics and Astronomy, Cardiff University, CF24 3AA, UK*
[*]*fortiz.huerta@gmail.com*

Abstract: For an efficient single-photon source a high-count rate into a well-defined spectral and spatial mode is desirable. Here we have developed a hybrid planar Fabry-Pérot microcavity by using a two-photon polymerization process (2PP) where coupling between single-photon sources (diamond colour centres) and resonance modes is observed. The first step consists of using the 2PP process to build a polymer table structure around previously characterized nitrogen-vacancy (NV) centres on top of a distributed Bragg reflector (DBR) with a high reflectivity at the NV zero-phonon line (ZPL). Afterwards, the polymer structure is covered with a silver layer to create a weak (low Q) cavity where resonance fluorescence measurements from the NVs are shown to be in good agreement with analytical and Finite Difference Time Domain (FDTD) results.

1. Introduction

Solid-state single-photon sources are considered one of the most promising candidates for single-photon emission [1]. Quantum dots (QDs) and colour centres in crystals are among the most studied, although colour centres in diamond such as NV and Silicon-Vacancy (SiV) centers have the main advantage of emitting single-photons at room-temperature, convenient for quantum photonic integration and applications. An ideal single-photon source should emit photons at a high-rate into a single mode, however, the rate of emission is limited by the spontaneous decay of the source and the light is emitted into the dipole emission pattern covering almost a full solid angle of 4π [2]. Different ways have been developed through the years to increase the emission rate and reduce the angle of emission of the sources [3]. Geometrical approaches exist, such as solid immersion lenses (SILs) [4,5] along with cavity quantum electrodynamics (CQED) approaches that rely on the Purcell enhancement by using resonant structures to selectively enhance emission into relevant modes [6,7]. Tunable Fabry-Pérot cavities with Bragg reflectors as mirrors [8–11] and photonic crystals [12–14] have also proved to be a viable option since small mode volumes can be achieved [15]. Using polymer to make structures for both approaches (geometrical and CQED) creates a new alternative for the realization of photonic and resonant devices of nearly arbitrary shape. By a process called two-photon polymerization (2PP), in which only the liquid polymer exposed to a specific wavelength gets solidified, solid immersion lenses [16] and resonant disks [17] have been fabricated with quantum dots and nanodiamonds inside the structures, respectively. These polymer structures hold the potential for the realization of a fully integrated quantum optical

#342904 https://doi.org/10.1364/OE.26.033245
Journal © 2018 Received 22 Aug 2018; revised 5 Oct 2018; accepted 12 Oct 2018; published 6 Dec 2018

Optics EXPRESS

chip incorporating single photon-emitters, SILs, resonant cavities, polymer waveguides [18] and polymer photonic crystals [19,20].

Here we present a new approach to build rapid and low-cost Fabry-Pérot cavities (with colour centres inside) combining the advantages of polymers, such as the ability to fabricate any geometrical shape desired, with the high-reflectivity of DBRs and metals to form a "hybrid" microcavity. The advantages and limitations of the newly developed hybrid Fabry-Pérot microcavities will also be mentioned.

2. Experimental setup

To find and characterize NV centres, we worked with a homebuilt confocal microscope [Fig. 1(a)]. The excitation beam consists of a *Ventus* $(532\,nm\,wavelength)$ continuous wave laser which is directed through a beam expander to collimate the beam and fill the back aperture of the objective. A silver mirror and a beamsplitter $(10:90)$ both redirect the incident beam onto the microscope objective $(0.9\,NA)$ which focuses the excitation light onto the sample that consists of DBR substrate coated with clusters of nanodiamonds containing NV centres. The substrate is attached to a piezo stage (tritor 101 SG controlled by a EDA3 from piezosystem jena) where the focused laser will raster scan typically around a 80x80 μm area [Fig. 1(b)]. The arriving counts can also be spectrally decomposed [Fig. 2(a)] through a spectrograph (Andor Solis, *Shamrock 163*) connected to a *CCD* camera (Andor Solis, *Newton)*. We added a Hanbury Brown-Twiss (HBT) setup to our confocal microscope [Fig. 1(a)] to measure the second order correlation function of our single-photon sources [Fig. 2(b)]. A delay box (*Model DB463,* Ortec) is also added to one of the arms to compensate for electronic dead times, and the coincidence counts are taken with a time correlated single photon counting (*TCSPC)* module (*PicoHarp 300, PicoQuant GmbH*).

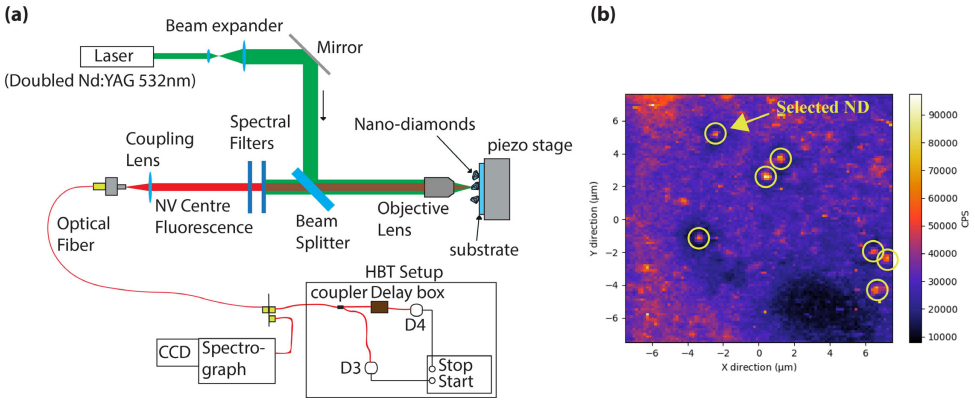

Fig. 1. (a) Confocal microscopy setup raster-scans nanodiamonds located on top of a substrate. Spectral and spatial filtering is applied to detect exclusively the NV fluorescence. The HBT setup measures coincidence counts at detectors D3 and D4 (SPCM-AQRH-14-FC). (b) A $15\times15\,\mu m$ scan allows visibility of NV centres (inside yellow circles). Scan made with a $0.15\,\mu m$ stepsize and $10\,s$ integration time.

An array of nanodiamonds (NDs) from Microdiamant was dropcast on top of a DBR, centered at $670\,nm$ with 15-pairs of alternating layers (Ta_2O_5 / SiO_2), to improve the collection efficiency of the NVs emission towards the objective lens through enhanced reflection of the surface of the DBR [Fig. 1(a)]. A clear antibunching behavior is shown in Fig. 2(b) where the second-order correlation function gives $g^{(2)}(0)<1$, indicating the presence of quantum emission [21] for the selected nanodiamond. Our $g^{(2)}(\tau)$ is defined as [22]:

Optics EXPRESS

$$g^{(2)}(\tau) = C_N(\tau) - (1-\rho^2)/\rho^2, \quad (1)$$

where $C_N(\tau)$ is the normalized coincidence counts and $\rho = S/(S+B)$ contains the signal (S) to background (B) ratio measured by the count rate next to the ND. We measured a $g^{(2)}(0) = 0.7,$ suggesting that more than one NV is being excited simultaneously inside the nanodiamond. A total of 102 kcounts/sec were detected for the selected ND [Fig. 2], with an excitation power of $170\,\mu W$ before the objective. The ND-dimension is small compared to the wavelength $(\sim 30\,nm)$ thus although there are likely 2-3 NVs inside the particle each can be thought of an individual dipole [23] located at the same position in the intracavity field. We then expect similar enhancement or inhibition of the fluorescence from each dipole due to this intracavity field [24,25].

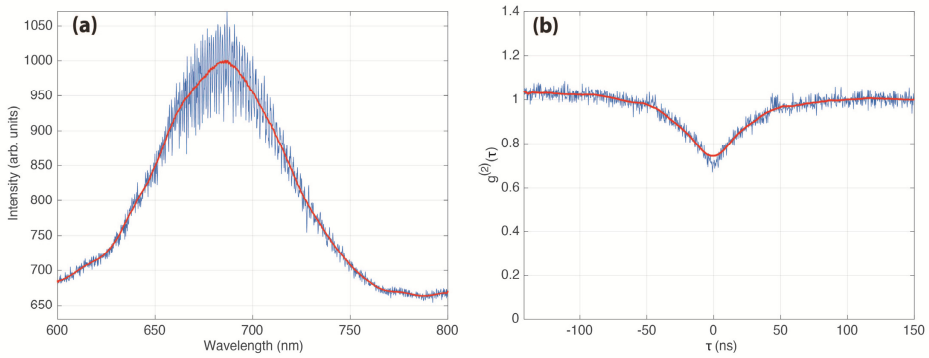

Fig. 2. (a) Blue: Fluorescence spectrum of selected ND measured with our confocal microscope. Red: Smoothed data (b) Blue: Antibunching behaviour of selected ND showing a $g^{(2)}(0) < 1$ with a timebin of $0.25\,ns$. Red: Smoothed data.

3. Fabrication and measurements

The printing of 3D micro-structures with a commercially available direct laser writing system (Photonic Professional, Nanoscribe GmbH) uses the 2PP process [Fig. 3(a)].

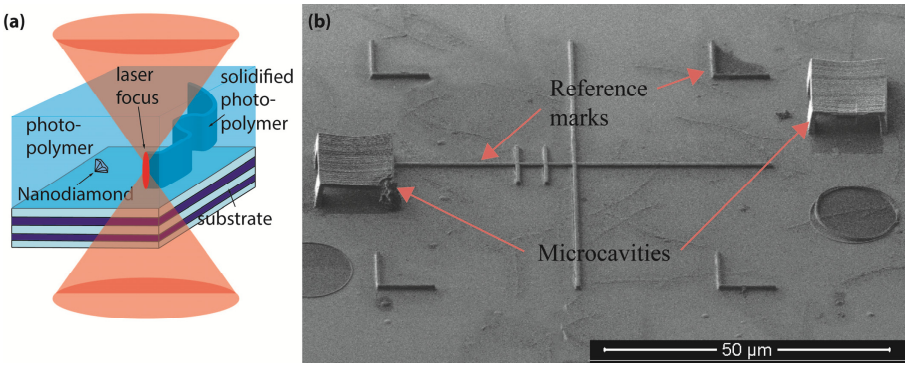

Fig. 3. (a) 2PP process, where the polymer exposed to the focal volume of the excitation beam (red) gets solidified through a two-photon absorption process. (b) Reference marks and two hybrid planar microcavities made with the 2PP process.

This method consists of illuminating a liquid photopolymer photoresist with light at 780 nm. When the photopolymer absorbs two photons simultaneously it triggers a chemical reaction that starts the solidification of the material.

Optics EXPRESS

As our next step, through a 2PP process, we built a polymer 'roof' of $15\times15\,\mu m$ with 4 polymer pillars [Fig. 4(a)] to hold it at a determined height on top of the pre-selected ND [Fig. 1(b)]. Reference marks were previously made on top of the DBR [Fig. 3(b)] (also with the 2PP process) to localize and mark the position of the pre-selected ND. Afterwards we added a silver layer of 20 nm (thermal evaporative deposition) on top of our polymer to end up with a fully-developed hybrid Fabry-Pérot cavity with a ND inside [Fig. 4].

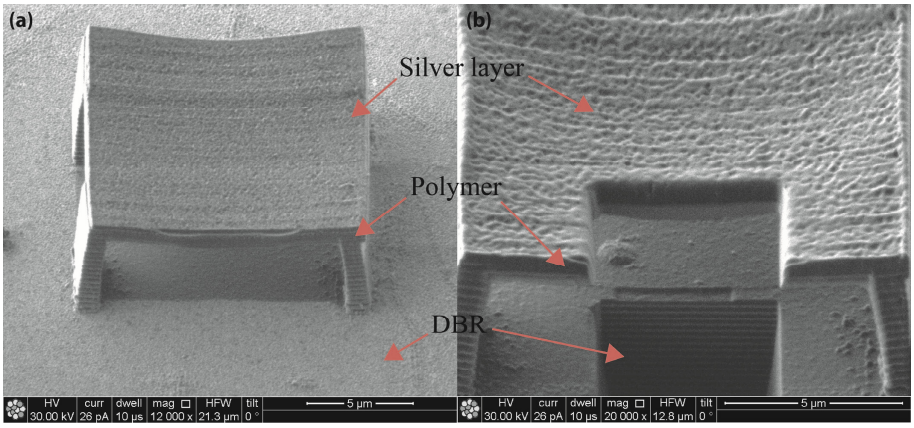

Fig. 4. (a) A FIB image of a hybrid Fabry-Pérot microcavity, (b) Cross-section of hybrid microcavity shows a thickness of ~800nm for the polymer/silver layer. The transversal cut also reveals the alternating layers of the DBR.

White light reflectivity spectral measurements [Fig. 5] for the hybrid planar cavity and substrate DBR was made with a home-built Fourier imaging spectroscopy system, which uses a high NA lens (0.75) to focus on samples and performs angular spectrum measurements as per angle [19]. Reflection at normal incidence was measured with a white light source and a spot size of $2.5\,\mu m$ therefore showing the resonant modes of our hybrid microcavity [Fig. 5(a)].

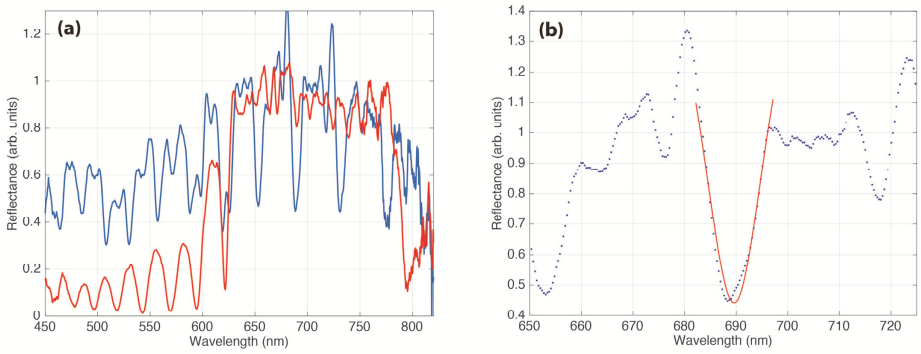

Fig. 5. (a) Blue: White light reflectance spectrum of hybrid planar microcavity with a FSR = 25 THz. Red: White light spectrum of DBR used as substrate for NDs. (b) Lorentzian fit (red) to a resonant dip (blue) with a FWHM = 17.3 nm and Q = 40.

Figure 5(b) shows one of the resonance dip features measured [cf. Figure 6(a)] which can be fitted using a Lorentzian function [11]. The full-width at half-maximum (FWHM) criteria then defines a quality factor (value associated with the loss of a resonator) of $Q=\lambda_0/\Delta\lambda$ for optical microcavities [26], where $\lambda_0=689\,nm$ is a resonance cavity mode and $\Delta\lambda=17.3\,nm$ [Fig. 5(b)] its spectral linewidth (FWHM). A value of $Q=40$ is measured for the hybrid

Optics EXPRESS

planar microcavity. Surface roughness [Fig. 4(b)] and absorption from the solidified polymer [27] diminishes the Q-factor of our cavity and therefore broadened the FWHM of the resonance modes [Fig. 5(b)]. Using illumination over a small area $(2.5\,\mu m)$ and at these low Q-values we expect only small effects on measured linewidths from the slight curvature of the top mirror evident in Fig. 4. A free spectral range (frequency separation between successive longitudinal modes) of $FSR = 25THz$ was measured from Fig. 5(a) and a total cavity length of $L_{total} = 6\mu m$ is calculated from $FSR = c/2L_{total}$ [26], where c is the lightspeed in vacuum.

Finally, in contrast with the preliminary results [Fig. 2(a)], we measured the fluorescence of the pre-selected quantum emitter, showing now a resonant behavior [Fig. 6(a)] due to the hybrid planar cavity where the peaks shown are the actual resonant modes of the cavity. Figure 6(a) also shows FDTD simulations in order to compare the experimental performance of the structures to an idealized performance. For these FDTD simulations performed, the polymer was treated as a lossless and non-dispersive dielectric so they don't take into account losses due to absorption or scattering due to surface roughness of the dielectric. We use a thickness of $L_2 = 770\,nm$, $L_{silver} = 20\,nm$ and $L_{1,FDTD} = 4.80\,\mu m$ for the polymer (index of refraction $n_2 = 1.52$), silver layer and the air-gap ($n_1 = 1$), respectively [Fig. 7(a)]. The thickness for the polymer/silver layers measured experimentally for the planar microcavity shows a value of $816.5\,nm \pm 103.5\,nm$ and an air-gap thickness of $L_{1,exp} = 4.75\,\mu m \pm 0.25\,\mu m$. Here there is broadening of the fluorescence enhancement due to the wide angle of emission and the slight curvature of the upper mirror.

The FDTD simulation was restricted to a dipole parallel to the DBR in a $5x5\,\mu m$ planar cavity for a reasonable computation time. Moreover, a $g^{(2)}$ measurement was also made on the pre-selected emitter [Fig. 6(b)]. A similar excitation power was used to obtain this measurement, however, the cavity is not resonant at the excitation wavelength, and therefore much of the incident light is reflected at the silver mirror. Hence, count rate from the NV centre is reduced while extra background is seen from the polymer and silver layers. Thus the $g^{(2)}$ measurement is highly noisy and difficult to correct from background but a reduced visibility antibunching signal can still be seen.

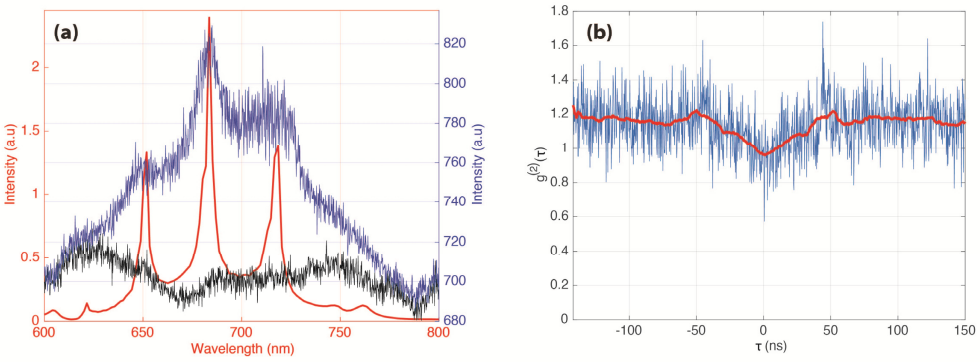

Fig. 6. (a) Blue: Fluorescence spectrum of pre-selected ND inside hybrid planar microcavity. Resonant peaks due to coupling to modes of cavity are shown. Visible resonant peaks at: 620 nm, 650 nm, 683.1 nm and 723.5 nm. Red: FDTD simulation of hybrid planar microcavity. Black: Background fluorescence of substrate measured next to ND. (b) Blue: Antibunching measurement from pre-selected ND inside cavity. Red: Smoothed data.

Optics EXPRESS

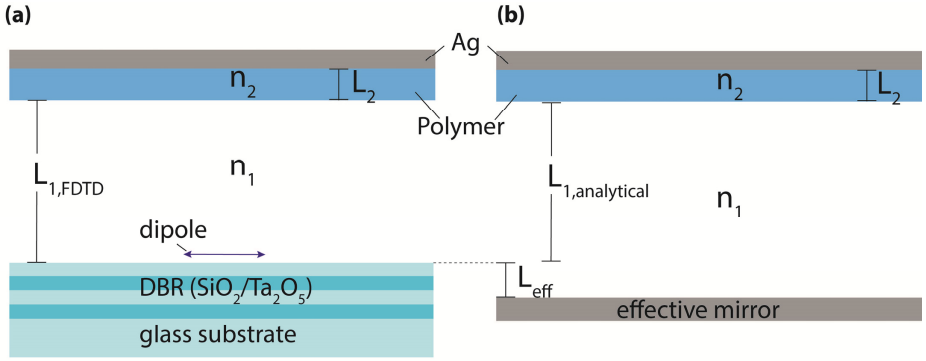

Fig. 7. (a) Cross-section of hybrid planar microcavity with a dipole parallel to the DBR surface for FDTD simulations (b) Effective mirror model used for analytical calculations of the resonant modes.

4. Analytical model

We also compared our experimental results with an analytical model [Table 1], where its main advantage relies on its simplicity to find the resonant modes of our cavity. For the analytical model, we use the resonant condition for a stable cavity [28], considering the extra phase shift $(k_2 L_2)$ introduced by the polymer and using the effective mirror model [Fig. 7(b)] for the DBR [29] we found the total phase shift in our cavity for a one-way trip to be:

$$k_1\left(L_{1,analytical}+L_{eff}\right)+k_2L_2-k_BL_{eff}=q\pi, \tag{2}$$

where $k_{1,2}=\omega n_{1,2}/c$ is the propagation constant of the resonant modes inside medium $n_{1,2}$, ω are the calculated resonant frequencies and c is the lightspeed in vacuum. According to the effective mirror model, the term $k_B=2\pi n_1/\lambda_B$, where $\lambda_B=670\,nm$ is the Bragg wavelength, must be added to ensure that the phase shift of a resonant mode at exactly the Bragg frequency is independent of the effective length L_{eff} of our mirror model. The value q is an integer number, $L_{1,analytical}=4.66\,\mu m$ is the air-gap thickness value used within the uncertainty of $L_{1,exp}$ and $L_{eff}=0.34\,\mu m$ is the effective length calculated by [30]:

$$L_{eff}=\frac{\lambda_B}{4\Delta n}, \tag{3}$$

where $\Delta n=\left|n_b-n_a\right|$ is the difference of index of refraction for the DBR alternating layers.

Table 1. Comparison table for analytical, FDTD and measured resonant frequencies

Measured (nm)	FDTD (nm)	Analytical (nm)
620	621	617
650	656	649
683.1	683	685
723.5	718	725

Optics EXPRESS

5. Conclusions

In summary, we have shown the fabrication steps for a hybrid planar microcavity deterministically placed around a pre-selected ND where FDTD and analytical results are in good agreement with the measured resonant modes, giving confidence on the resonant nature of our cavities. This simple analytical model could also be used, by fine-tuning the height of the cavity $\left(L_{1,analytical}\right)$ and polymer thickness $\left(L_2\right)$, to find the desired resonant modes prior to the fabrication process of the cavity.

However, polymer, known for its malleability, still presents challenges for the fabrication of photonic integrated optical structures, where scattering and absorption challenges must be overcome in order to increase the optical quality of our hybrid microcavities. Post-processing of the cavities (e.g. focused ion beam nano-polishing) could be applied to minimize these issues. A direct comparison of the pre-selected ND fluorescence before and after the fabrication process of the cavity reassures the resonance behaviour predicted by the white light spectral measurements of Fig. 5. To the best of our knowledge, this is the first example of the use of 2PP lithography to fabricate a hybrid planar Fabry-Pérot microcavity showing evidence of resonance fluorescence even with a weak (low-Q) resonant cavity. This fabrication process opens new possibilities for more exotic structures for the emission enhancement of single-photon sources.

Funding

Engineering and Physical Sciences Research Council grant (EPSRC) (EP/M024458/1, EP/M009033/1); European Research Council advanced grant (ERC) (247462 QUOWSS).

Acknowledgments

2PP was carried out using the nanofabrication equipment of the Centre for Nanoscience and Quantum Information, University of Bristol, Bristol, UK. We acknowledge Dr. Peter Heard and Dr. Andrew Murray, assisted with FIB milling and metal deposition in the University of Bristol Cleanroom. FOH acknowledges financial support from CONACYT.

References

1. I. Aharonovich, D. Englund, and M. Toth, "Solid-state single-photon emitters," Nat. Photonics **10**(10), 631–641 (2016).
2. S. Prawer and I. Aharonovich, *Quantum Information Processing with Diamond: Principles and Applications* (Elsevier, 2014).
3. W. L. Barnes, G. Björk, J. M. Gérard, P. Jonsson, J. A. E. Wasey, P. T. Worthing, and V. Zwiller, "Solid-state single photon sources: Light collection strategies," Eur. Phys. J. D **18**(2), 197–210 (2002).
4. J. P. Hadden, J. P. Harrison, A. C. Stanley-Clarke, L. Marseglia, Y. L. D. Ho, B. R. Patton, J. L. O'Brien, and J. G. Rarity, "Strongly enhanced photon collection from diamond defect centers under microfabricated integrated solid immersion lenses," Appl. Phys. Lett. **97**(24), 241901 (2010).
5. T. Schröder, F. Gädeke, M. J. Banholzer, and O. Benson, "Ultrabright and efficient single-photon generation based on nitrogen-vacancy centres in nanodiamonds on a solid immersion lens," New J. Phys. **13**(5), 055017 (2011).
6. R. Albrecht, A. Bommer, C. Pauly, F. Mücklich, A. W. Schell, P. Engel, T. Schröder, O. Benson, J. Reichel, and C. Becher, "Narrow-band single photon emission at room temperature based on a single nitrogen-vacancy center coupled to an all-fiber-cavity," Appl. Phys. Lett. **105**(7), 073113 (2014).
7. A. Muller, E. B. Flagg, J. R. Lawall, and G. S. Solomon, "Fabry – Perot microcavity," **35**, 2293–2295 (2010).
8. T. W. Allen, J. Silverstone, N. Ponnampalam, T. Olsen, A. Meldrum, and R. G. DeCorby, "High-finesse cavities fabricated by buckling self-assembly of a-Si/SiO2 multilayers," Opt. Express **19**(20), 18903–18909 (2011).
9. D. Hunger, T. Steinmetz, Y. Colombe, C. Deutsch, T. W. Hänsch, and J. Reichel, "A fiber Fabry-Perot cavity with high finesse," New J. Phys. **12**(6), 065038 (2010).
10. J. Benedikter, T. Hümmer, M. Mader, B. Schlederer, J. Reichel, T. W. Hansch, and D. Hunger, "Transverse-mode coupling and diffraction loss in tunable Fabry-Pé rot microcavities," New J. Phys. **17**(5), 053051 (2015).
11. P. R. Dolan, G. M. Hughes, F. Grazioso, B. R. Patton, and J. M. Smith, "Femtoliter tunable optical cavity arrays," Opt. Lett. **35**(21), 3556–3558 (2010).
12. A. Faraon, C. Santori, Z. Huang, V. M. Acosta, and R. G. Beausoleil, "Coupling of nitrogen-vacancy centers to photonic crystal cavities in monocrystalline diamond," Phys. Rev. Lett. **109**(3), 033604 (2012).

Optics EXPRESS

13. J. C. Lee, D. O. Bracher, S. Cui, K. Ohno, C. A. McLellan, X. Zhang, P. Andrich, B. Alemán, K. J. Russell, A. P. Magyar, I. Aharonovich, A. Bleszynski Jayich, D. Awschalom, and E. L. Hu, "Deterministic coupling of delta-doped nitrogen vacancy centers to a nanobeam photonic crystal cavity," Appl. Phys. Lett. **105**(26), 261101 (2014).
14. A. Sipahigil, R. E. Evans, D. D. Sukachev, M. J. Burek, J. Borregaard, M. K. Bhaskar, C. T. Nguyen, J. L. Pacheco, H. A. Atikian, C. Meuwly, R. M. Camacho, F. Jelezko, E. Bielejec, H. Park, M. Lončar, and M. D. Lukin, "An integrated diamond nanophotonics platform for quantum-optical networks," Science **354**(6314), 847–850 (2016).
15. K. J. Vahala, "Optical microcavities," Nature **424**(6950), 839–846 (2003).
16. M. Sartison, S. L. Portalupi, T. Gissibl, M. Jetter, H. Giessen, and P. Michler, "Combining in-situ lithography with 3D printed solid immersion lenses for single quantum dot spectroscopy," Sci. Rep. **7**(1), 39916 (2017).
17. A. W. Schell, J. Kaschke, J. Fischer, R. Henze, J. Wolters, M. Wegener, and O. Benson, "Three-dimensional quantum photonic elements based on single nitrogen vacancy-centres in laser-written microstructures," Sci. Rep. **3**(1), 1577 (2013).
18. Q. Shi, B. Sontheimer, N. Nikolay, A. W. Schell, J. Fischer, A. Naber, O. Benson, and M. Wegener, "Wiring up pre-characterized single-photon emitters by laser lithography," Sci. Rep. **6**(1), 31135 (2016).
19. L. Chen, M. Lopez-Garcia, M. P. C. Taverne, X. Zheng, Y. D. Ho, and J. Rarity, "Direct wide-angle measurement of a photonic band structure in a three-dimensional photonic crystal using infrared Fourier imaging spectroscopy," Opt. Lett. **42**(8), 1584–1587 (2017).
20. L. Chen, M. P. C. Taverne, X. Zheng, J.-D. Lin, R. Oulton, M. Lopez-Garcia, Y.-L. D. Ho, and J. G. Rarity, "Evidence of near-infrared partial photonic bandgap in polymeric rod-connected diamond structures," Opt. Express **23**, 26565–26575 (2015).
21. R. Loudon, *The Quantum Theory of Light* (OUP Oxford, 2000).
22. A. Beveratos, S. Kühn, R. Brouri, T. Gacoin, J. P. Poizat, and P. Grangier, "Room temperature stable single-photon source," Eur. Phys. J. D **18**(2), 191–196 (2002).
23. H. Kaupp, T. Hümmer, M. Mader, B. Schlederer, J. Benedikter, P. Haeusser, H. C. Chang, H. Fedder, T. W. Hänsch, and D. Hunger, "Purcell-Enhanced Single-Photon Emission from Nitrogen-Vacancy Centers Coupled to a Tunable Microcavity," Phys. Rev. Appl. **6**(5), 054010 (2016).
24. L. Novotny, *Principles of Nano-Optics* (Cambridge University Press, 2007).
25. C. Lei, D. G. Deppe, Z. Huang, and C. C. Lin, "Emission Characteristics From Dipoles with Fixed Positions in Fabry-Perot Cavities," IEEE J. Quantum Electron. **29**(5), 1383–1386 (1993).
26. M. C. Teich and B. Saleh, "Fundamentals of photonics," Canada, Wiley Intersci. **3**, (1991).
27. G. H. Meeten, *Optical Properties of Polymers* (Elsevier Appl. Sci. Publ. Ltd, 1986).
28. A. E. Siegman, *Lasers* (University Science Books, 1986).
29. D. I. Babic and S. W. Corzine, "Analytic Expressions for the Reflection Delay, Penetration Depth, and Absorptance of Quarterwave Dielectric Mirrors," IEEE J. Quantum Electron. **28**(2), 514–524 (1992).
30. C. W. Wilmsen, H. Temkin, and L. A. Coldren, "Vertical-cavity surface-emitting lasers," in Vertical-*Cavity Surface-Emitting Lasers*, C. W. Wilmsen, H. Temkin, and L. A. Coldren, eds. (Cambridge University Press, 1999), pp. 474.